Amyloid-like Hfq interaction with single stranded DNA: involvement in recombination and replication in *Escherichia coli*

Running title: Hfq:single stranded DNA interaction

Krzysztof Kubiak[1,2], Frank Wien[3], Indresh Yadav[4], Nykola C. Jones[5], Søren Vrønning Hoffmann[5], Eric Le Cam[6], Antoine Cossa[2,7], Frederic Geinguenaud[8], Johan R. C. van der Maarel[4], Grzegorz Węgrzyn[1]* and Véronique Arluison[2,9]*

[1] *Department of Molecular Biology, University of Gdansk, Wita Stwosza 59, 80-308 Gdansk, Poland*

[2] *Laboratoire Léon Brillouin, Université Paris Saclay, CEA, CNRS, LLB, 91191 Gif-sur-Yvette, France*

[3] *DISCO Beamline, Synchrotron SOLEIL, 91192 Gif-sur-Yvette, France*

[4] *Department of Physics, National University of Singapore, Singapore 117542, Singapore*

[5] *ISA, Department of Physics and Astronomy, Aarhus University, 8000 Aarhus C, Denmark*

[6] *UMR9019-CNRS, Genome Integrity and Cancer, Université Paris-Saclay, Gustave Roussy, F-94805, Villejuif Cedex, France*

[7] *Institut Curie, PSL University, Université Paris-Saclay, CNRS UMS2016, Inserm US43, Multimodal Imaging Centre, 91400 Orsay, France*

[8] *Plateforme CNanoMat and Inserm, U1148, Laboratory for Vascular Translational Science, UFR SMBH, Université Paris 13, Sorbonne Paris Cité, F-93017, Bobigny, France*

[9] *Université Paris Cité, UFR SDV, 75006 Paris, France*

* Co-corresponding authors: Véronique Arluison; Tel 33 (0)1 69 08 32 82; veronique.arluison@u-paris.fr Grzegorz Węgrzyn; Tel +48 58 523 6024; grzegorz.wegrzyn@biol.ug.edu.pl

This peer-reviewed article has been accepted for publication but not yet copyedited or typeset, and so may be subject to change during the production process. The article is considered published and may be cited using its DOI.

10.1017/qrd.2022.15

ABSTRACT

Interactions between proteins and single stranded DNA (ssDNA) are crucial for many fundamental biological processes, including DNA replication and genetic recombination. Thus, understanding detailed mechanisms of these interactions is necessary to uncover regulatory rules occurring in all living cells. The RNA-binding Hfq is a pleiotropic bacterial regulator that mediates many aspects of nucleic acids metabolism. The protein notably mediates mRNA stability and translation efficiency by using stress-related small regulatory RNA as cofactors. In addition, Hfq helps to compact double stranded DNA. In this paper, we focused on the action of Hfq on ssDNA. A combination of experimental methodologies, including spectroscopy and molecular imaging, have been used to probe the interactions of Hfq and its amyloid C-terminal region with ssDNA. Our analysis revealed that Hfq binds to ssDNA. Moreover, we demonstrate for the first time that Hfq drastically changes the structure and helical parameters of ssDNA, mainly due to its C-terminal amyloid-like domain. The formation of the nucleoprotein complexes between Hfq and ssDNA unveil important implications for DNA replication and recombination.

Keywords

Single strand DNA binding protein; bacterial amyloid; Sm-like protein; Hfq; noncoding RNA; nucleoid associated protein

https://doi.org/10.1017/qrd.2022.15 Published online by Cambridge University Press

Introduction

Although most genetic information is stored in double-stranded dsDNA, genetic expression requires unwinding of DNA into single-stranded ssDNA. In particular, transient portions of ssDNA appear during replication, recombination or repair processes; ssDNA is more sensitive to nuclease degradation and this leads to the formation of secondary structures, which prevent previously cited processes. To solve these problems, cells need specialized ssDNA-binding proteins SSB that bind and stabilize ssDNA structures. These proteins usually do not share significant sequence similarity, but all contain a DNA-binding oligonucleotide binding OB fold (Su et al., 2014), consisting of a five-stranded curved β sheet capped by a helix. This specific fold is responsible for ssDNA binding, but also often for the self-assembly of oligomeric SSB. In bacterial cells, ssDNA fragments also play crucial roles, including nucleoid and phage DNA replication or genetic recombination (Molan & Zgur Bertok, 2022).

In bacterial chromosome replication, ssDNA regions are necessary for initiating the process of DNA synthesis by melting the double helix, recruiting the multiprotein machinery, and allowing formation of primers and replication forks (Zawilak-Pawlik et al., 2017). Therefore, proteins interacting with ssDNA and/or stabilizing such DNA fragments, like the single-strand DNA-binding protein, play important roles in facilitating the formation of nucleoprotein complexes at replication forks and maintaining their functions (Oakley, 2019). Bacterial proteins that interact with such DNA structures particularly affect replication of viruses, including bacteriophages, having genomes composed of ssDNA (Shulman & Davidson, 2017). The transition from ss to dsDNA is a crucial step in propagation of such viruses, thus, proteins interacting with ssDNA can significantly modulate the viral replication processes.

Another process in which ssDNA is crucial is homologous recombination. DNA strand displacement and replacement occurring in this process, require the formation of complexes including ssDNA and specific proteins (Piazza & Heyer, 2019), and the influence of ssDNA-interacting proteins may be important in modulating recombination efficiency. The function of the bacteriophage λ Red recombination system may serve as an example of such a ssDNA-dependent process (Sharan et al., 2009). In summary, proteins interacting with ssDNA may influence various biological processes, and thus, one should consider that any ssDNA-binding protein might modulate chromosomal and viral replication, as well as genetic recombination.

https://doi.org/10.1017/qrd.2022.15 Published online by Cambridge University Press

In this work we focused our attention on the ssDNA binding property of the *Escherichia coli* Hfq protein. Hfq is an abundant protein that flexibly binds nucleic acids (NA) (Rajkowitsch & Schroeder, 2007; Vogel & Luisi, 2011). Structurally, the amino-terminal region of Hfq (NTR, 65 residues) shares homologies with the Sm family of protein (Wilusz & Wilusz, 2013) adopting the OB-like fold. Hfq-NTR is comprised of five β-strands and another Sm-proteins assembles into a cyclic oligomer to form the functional unit (Brennan & Link, 2007). Although the mechanism by which Hfq binds NA is not completely clear, it is now established that its NTR binds RNA and DNA. Uridine-rich RNA are bound to one face of the torus called the proximal face, while the A-rich sequences bind to the opposite distal face; dsDNA is also bound on the proximal face of the ring (Sup. Fig. S1) (Link et al., 2009; Orans et al., 2020).

In addition to the well-characterized Sm domain, the Hfq protein also possesses a C-terminal region (CTR, 40 residues) located at the periphery of the torus (Arluison et al., 2004). Although no atomic 3D structure is known for the CTR, it has been shown to self-assemble into an amyloid structure (Fortas et al., 2015). Recently, it has been suggested that the CTR collaborates with the different RNA binding faces of Hfq, with important outcomes for some RNAs (Kavita et al., 2022).

Functionally, Hfq controls a large number of bacterial functions. Among them, most are related to RNAs. Hfq was first identified as a host-factor for a RNA bacteriophage, but later found to play a general role in RNA metabolism (Vogel & Luisi, 2011). In particular, it facilitates the pairing of small non-coding RNA (sRNA) with target mRNA, allowing gene regulation at the post-transcriptional level. Indeed, Hfq allows a tight and fast regulation of gene expression and triggers stress-relief pathways (Gottesman, 2019).

Interestingly, Hfq also binds to DNA (Cech et al., 2016) and some of the phenotypic effects appearing due to the lack of Hfq may be linked to defects in DNA-related processes. Hfq binds both linear and circular dsDNA (Takada et al., 1997) and a significant amount of the protein is found in the nucleoid (~20%) (Diestra et al., 2009). Hfq binding results in the condensation of DNA through protein-protein interactions. This activity, consisting of the mediation of nucleic acid interactions and referred to as bridging, is observed for other nucleoid associated proteins to form loops (Rajkowitsch & Schroeder, 2007; Wiggins et al., 2009).

The compaction of DNA by Hfq *in vitro* is mainly due to its CTR (Malabirade et al., 2017a). Thus, Hfq probably plays a critical role in the architecture of the chromosome, even if this has not been established formally. If Hfq does not affect DNA supercoiling and transcription directly (Malabirade

https://doi.org/10.1017/qrd.2022.15 Published online by Cambridge University Press

et al., 2018), it possibly regulates them indirectly, for instance by regulating the expression of a transcriptional regulator (Majdalani et al., 1998).

The work reported here further explores a newly discovered property of Hfq, its ability to bind ssDNA and to drastically change ssDNA structure by promoting its alignment. Effects of Hfq on DNA transactions in which ssDNA regions are crucial have been assessed.

Methods

Details of methods can be found online as Supplementary Material.

Protein expression and purification

Wild type and truncated Hfq forms of *E. coli* Hfq were purified as described previously (Malabirade et al., 2017b; Taghbalout et al., 2014). CTR peptide was chemically synthetized. This part of the protein cannot be purified from bacteria as it is unstable when translated alone (Taghbalout et al., 2014). We determined that the pH~5 used was the most appropriate to form the complex with DNA. Although pH 5 seems to be far from physiological conditions, it is still relevant as Gram-negative bacteria can acidify their cytosol when adapting to the vacuoles of the host macrophage, and many virulent genes belong to the Hfq regulon in these bacterial species (Kenney, 2019).

Fluorescence anisotropy measurements

Fluorescence anisotropy measurements were collected as described previously (Geinguenaud et al., 2011).

Optical Microscopy of ssDNA-Hfq/CTR/NTR Complexes

DNA in the single-stranded form was prepared by alkali-induced denaturation of double-stranded λ-DNA (Basak et al., 2019). Then, Hfq (29.8 μM) was added to the solution with concentration of one hexamer-Hfq per 200 bases. A similar procedure was used to make the ssDNA with Hfq-CTR and Hfq-NTR. However, the molar concentration of CTR used was six times higher than Hfq, i.e. 6 CTR for 200 bases of DNA. For fluorescence imaging, one hour before imaging, ssDNA was stained with YOYO-1 at a concentration of one YOYO-1 dye per four bases.

Synchrotron Radiation Circular and Linear Dichroism (SRCD and SRLD)

https://doi.org/10.1017/qrd.2022.15 Published online by Cambridge University Press

Complex between dA_{59} and Hfq-CTR was prepared as described previously (El Hamoui et al., 2020). SRCD measurements were carried out at DISCO/SOLEIL Synchrotron (proposal 20200007). Samples were loaded into a CaF_2 circular cell (24 µm pathlength). Due to the origin of absorption, spectra of mixed samples could not be standardized to $\Delta\varepsilon$ and spectra are presented in mdeg maintaining the same molar ratios for all presented samples. SRLD measurements were carried out in the same cell by collecting triplicates every 90° from 0-270°. For the data-acquisition the modulator phase was set to λx0.608 doubling the lock-in amplifier frequency in order to measure only LD absorption.

Couette flow Synchrotron Radiation Linear Dichroism

Couette flow SRLD measurements were performed at the AU-CD beamline on the ASTRID2 synchrotron (proposal ISA-21-102), as detailed in (Wien et al., 2019). Due to the much larger path length of the Couette flow cell used for SRLD measurements (0.5 mm) compared to the path length used for SRCD measurements (0.024 mm), the complex between CTR and the dA_{59} had a very strong LD signal under flow conditions; the samples where diluted (1/36) compared to the concentrations used for SRCD.

Fourier Transform Infrared spectroscopy (FTIR)

For FTIR analysis, the same solutions used for SRCD analysis were lyophilized and re-dissolved in D_2O (5 µL). FTIR measurements were performed as detailed in (Geinguenaud et al., 2011).

TEM imaging

3.65 nM circular ssDNA molecules extracted from ΦX174 virions was incubated with 100 nM CTR in Tris-HCl 10 mM pH7.5 EDTA 1 mM for 10 minutes at 20°C. 5 µl were then deposited onto positively functionalized grids covered with a thin carbon film (Beloin et al., 2003). Grids were washed with aqueous 2% (w/v) uranyl acetate, dried and observed in annular darkfield mode using a Zeiss 902 EM. Veletta CCD camera is controlled by iTEM software (Olympus Soft Imaging).

E. coli strains and bacteriophages

E. coli wild-type strain MG1655 (Jensen, 1993) was used as the *hfq*$^+$ positive control. Its Δ*hfq* and ΔCTR derivatives were constructed as described in (Gaffke et al., 2021). Quantification of Hfq and its CTR-truncated form was by Western-blotting and confirmed by dot-blotting. For propagation of bacteriophage M13, *hfq*$^+$, Δ*hfq* and ΔCTR derivatives of *E. coli* strain Hfr3000 (Bachmann, 1972)

https://doi.org/10.1017/qrd.2022.15 Published online by Cambridge University Press

were constructed by P1 transduction. Bacteriophages M13 (Salivar et al., 1964), λ*c*I857*S*7(am) (Goldberg & Howe, 1969), called λ*S*(am) in this work, and λ*b519imm21susP* (Wegrzyn et al., 1995), called λ*P*(am) in this work, were used. *E. coli* strain TAP90 (Patterson & Dean, 1987) was used for propagation and titration of phages λ*cI857S7*(am) and λ*b519imm21susP*.

Bacteriophage M13 development and efficiency of phage λ recombination

Development of phage M13 Phage λ recombination efficiency were tested according to the previously described method (Mosberg et al., 2010).

Results

Hfq binds, coats and spreads ssDNA

The potential of Hfq to bind to ssDNA was investigated. We chose $(dA)_n$ sequences because Hfq has the highest affinity for A-rich sequences (Folichon et al., 2003; Geinguenaud et al., 2011). Indeed, A-tracts are over-represented and distributed throughout the *E. coli* genome in phased A-repetitions (~ 12 nucleotides), organized in approximately 100 nucleotides-long clusters. (Tolstorukov et al., 2005). Titrations of dA_7, dA_{20} and dA_{59} with Hfq gave K_d values of 3.5±0.2 μM, 183±8 nM and 166±16 nM, respectively (Sup Fig. S2). A weaker affinity was measured for the CTR and dA_{59}, about 4.2±0.3 μM, thus suggesting that Hfq can bind dA_{59} using both its NTR and CTR regions, as previously observed for longer dsDNA (Jiang et al., 2015).

The coating of ssDNA by Hfq and its truncated forms was then tested. For this purpose, different approaches have been used. First DNA in its single-stranded form was prepared by alkali-induced denaturation of λ dsDNA. The ssDNA molecules were subsequently complexed with the protein following a buffer exchange according to the method previously reported (Basak et al., 2019). Prior to imaging using fluorescence microscopy, the complexes were stained with YOYO-1 dye. The fluorescence intensity is relatively weak, because for ssDNA the dye is side-bound and cannot intercalate. Two different types of experiments have been done: stretched on a surface and confined in a nanochannel. First, the coated molecules were analyzed on a flat surface (Allemand et al., 1997). The images are shown in Fig. 1A; the corresponding measured average stretches are also presented. As shown, the results are almost identical for Hfq, CTR or NTR. The ssDNA molecules are thus

https://doi.org/10.1017/qrd.2022.15 Published online by Cambridge University Press

almost fully stretched with a similar contour length of 25±2 μm (0.52 nm/base), irrespective of the protein or its truncated forms. This confirms that both the NTR and CTR bind and coat ssDNA. A second type of experiment was done using a nanofluidic device to mimic a confined environment. In this experiment, ssDNA coated with Hfq was brought inside a rectangular channel with a cross-sectional diameter of 125 nm using an electric field. Once the complexes are inside the channel, they were allowed to relax for two minutes before imaging. The stretch of the complexes in the longitudinal direction of the channel was measured and are shown in the histogram in Fig. 1-B. The corresponding histogram pertaining to the combing experiment has also been included. The mean stretch of the nano-confined complexes was found to be 15±2 μm, which results in a relative stretch of 0.6±0.1. In the case of naked dsDNA confined to the same channel, the relative stretch was reported to be 0.528±0.005 (Yadav et al., 2020). It must be emphasized that bare ssDNA without protein coating is notoriously difficult to linearize with molecular combing and cannot be stretched inside a nanochannel due to strong intramolecular hybridization. We conclude that the relative stretches of ssDNA coated with full-length Hfq and naked dsDNA confined to the 125 nm channel are similar, which indicates that the bending rigidity (persistence length) of the coated ssDNA filament is about the same as that of bare dsDNA. In contrast, previous reports with another method allowing imaging of naked ssDNA pointed to lower values with a wide variation for ssDNA extension*, i.e.* from 0.18 nm/base to 0.36 nm/base (Hansma et al., 1992; Woolley & Kelly, 2001), thus ssDNA extension by Hfq and its CTR (0.52 nm/base) is significantly more. Extension of ssDNA by Hfq and/or its CTR also exceeds the extension following coating of ssDNA with a cationic-neutral polypeptide copolymer (0.32 nm/base (Basak et al., 2019)). Note that in these experiments, the coated ssDNA molecules are aligned through the application of flow (combing) or confinement to a long and narrow channel. Although some intermolecular aggregation was observed, these aggregates generally break up due to the alignment procedure. Quantitative information regarding intermolecular bridging could, hence, not be obtained from these essentially single-molecule stretching experiments.

The effect of Hfq-CTR was then confirmed with Transmission Electron microscopy (TEM). This experiment was done with circular viral DNA (single-stranded) and not linear molecules (Fig 1C). Circular ssDNA molecules were deposited on a carbon surface previously functionalized with positive charges and positively stained. TEM clearly confirms the capability of CTR to spread some regions of the viral DNA in conjunction with folding of other regions by intra- or intermolecular

https://doi.org/10.1017/qrd.2022.15 Published online by Cambridge University Press

bridging interaction (Fig. 1C, sub-panels B1 and B2). Note that the relative alignment, parallel or antiparallel, of ssDNA portions in the bridged regions cannot be determined.

Hfq changes ssDNA structure and allows DNA alignment

Next, the effect of Hfq-CTR on ssDNA has been investigated using synchrotron radiation circular dichroism SRCD. We identified significant spectral changes over the whole spectrum (Fig. 2). Assuming that the protein is restructuring (amyloid formation) upon DNA binding (Malabirade et al., 2018), we also identified that the ssDNA structure changes. We note a positive band at 180 nm and a negative band at 190 nm both indicative of left-handed NA (Wien et al., 2021). In contrast, a positive band around 185 nm and a negative one between 200-210 nm is indicative of right-handed NAs (Wien et al., 2021). The spectral change identified could be correlated to base-tilting of A-rich sequences (Edmondson & Johnson, 1985; Wien et al., 2019). Furthermore, the influence of Hfq on the positive CD signal around 270 nm may be influenced by base pairing and stacking (Holm et al., 2010; Wien et al., 2021).

One possible explanation for the spectral inversion observed could be due to a change in helical parameters. To test this possibility, we used FTIR spectroscopy to analyze sugar puckering. When only C3'-endo sugars are present, characteristic absorption bands located at 865 and 820 cm^{-1} are observed, corresponding to the A-form. A contribution around 840 cm^{-1} is indicative of a C2'-endo conformation (B-form) (Wien et al., 2021). The formation of a Z-like form is excluded as it would give a triplet at 970, 951 and 925 cm^{-1} (Banyay et al., 2003). The A-form would give a triplet at 977, 968 and 952 cm^{-1} and the B form would give a singlet at 970 cm^{-1}. As shown in Fig. 3A, we clearly see that the d-ribose stays in C2'-endo since we observe the typical bands near 840 and 970 cm^{-1}. We thus conclude that ssDNA complexed to Hfq remains in B-form.

A possibility could be that the pH 5 used in our conditions could result in the formation of A^+ adenine and subsequently in a parallel helix (Gleghorn et al., 2016). FTIR analysis of our complex confirms this hypothesis: the band at 1658 cm^{-1} is absent in dA_{59} alone, but the shift from 932 to 947 cm^{-1} and the net decrease of the band intensity at 1080 cm^{-1} shows that a parallel helix is formed by dA_{59} when bound to CTR (Fig. 3B) (Taillandier & Liquier, 2002). This result is confirmed using SRCD as dA_{59} complexed to CTR exhibits a spectrum similar to that of poly(dA) parallel helix (Holm et al., 2012). We thus conclude the CTR induces the formation of ds parallel helix from ss dA_{59}. This is not the case for ssDNA alone; thus, the CTR promotes the formation of this parallel helix.

https://doi.org/10.1017/qrd.2022.15 Published online by Cambridge University Press

Next, as the formation of such a parallel helix could result in the alignment of ssDNA, we analyzed the possible alignment of the ssDNA molecule by CTR. Indeed, we previously observed that the CTR amyloid region has a propensity to align DNA (Wien et al., 2019). As shown in Fig. 4, a clear alignment by the CTR:ssDNA complex can also be observed under Couette flow conditions. The alignment without rotation in a flow cell was also confirmed by SRLD using a CD cell and a CD cell rotation chamber (Fig. 4C). Alignment of the complex in the CD sample may occur upon loading between short pathlengths, hence linear dichroism (LD) signals emerge. These signals, if strong enough, spill into the CD signal via LD-CD cross talk (Sutherland, 2009) and distort the CD spectrum. In order to eliminate the LD contribution acquisition of CD spectra at four angles (0°-90°-180°-270°) were averaged.

Shown in Fig. 4A are the SRLD spectra of CTR, ssDNA and finally of the complex CTR:dA_{59}. The LD signal is effectively zero for both Hfq-CTR and ssDNA compared to the very strong LD signal of the complex. This shows that although the two components do not align under flow conditions, the complex readily aligns. In contrast to the LD signal observed for dsDNA complexes with Hfq-CTR (Wien et al., 2019), we observe that the LD signal is positive for all wavelengths including the wavelength range from 240 to 300 nm where the DNA signal dominates. This leads to a surprising conclusion: where long DNA normally aligns along the flow direction giving rise to negative LD signals (Dicko et al., 2008), the parallel dsDNA formed by dA_{59} are incorporated into the polymers of the complex in such a way that they are aligned perpendicular to the length of the amyloid strand. The positive signal at 195 nm is in agreement with the β-sheet secondary structure aligned perpendicular to the amyloid fibrils and thus the flow (Wien et al., 2019) since β-strands have a transition dipole moment near 195 nm aligned perpendicular to the direction of the strand (Nordén et al., 2010).

In conclusion, our results clearly show that *in vitro* the Hfq protein, and in particular its CTR amyloid region, are able to bind to ssDNA, cover, spread and bridge it, and to allow the alignment of ssDNA molecules. Because ssDNA is an essential intermediate in many DNA metabolic processes, we then analyzed the effect of Hfq *in vivo* for two processes where ssDNA is formed. Hfq could indeed be part of the ssDNA-binding SSB protein family in prokaryotic cells, which bind to ssDNA, stabilizing and protecting intermediate states of DNA recombination and replication.

This could particularly be the case for A-rich sequences found throughout the *E. coli* genome and when pH decreases during host infection (Kenney, 2019; Tolstorukov et al., 2005). Furthermore, it

https://doi.org/10.1017/qrd.2022.15 Published online by Cambridge University Press

could prevent ssDNA chemical attack or be involved in removal of secondary structures that could impair ssDNA related processes (Molan & Zgur Bertok, 2022).

Hfq influences replication of bacteriophage M13 and genetic recombination

To evaluate if Hfq influences biological processes in which ssDNA regions are involved, we have tested efficiencies of M13-bacteriophage replication which has a ssDNA genome and genetic recombination between genomes of λ–bacteriophage (Red-recombination system).

When testing development of the M13 bacteriophage, we found that its efficiency is significantly more effective in the Δ*hfq* mutant relative to wild type WT control (Fig. 5A). Since effects observed in mutants completely devoid of Hfq might be caused by the absence of various activities of this protein, we repeated these experiments using a mutant with deletion of the Hfq CTR while leaving intact the NTR. In such a mutant, replication of the M13 phage was significantly less efficient relative to wild-type counterpart, as shown by slower phage development and lower burst size (Fig. 5A).

To test efficiency of genetic recombination, we have employed λ–bacteriophage mutants. Nonsense (amber, or shortly am) λ mutants in genes *P* or *S* can propagate only in suppressor *E. coli* hosts (*supE* and *supF*, respectively), but not in WT bacteria. When WT, Δ*hfq* or ΔCTR cells were infected simultaneously with both phage mutants, Red-recombination could occur. Culture-growth was timely stopped and phage lysates were prepared after one single lytic development cycle was reached. Thus, phage progeny contained parental phages and recombinants, including λ*P*(am)*S*(am) and $\lambda P^{+}S^{+}$ variants. The latter phages could be easily distinguished from parental viruses because of their ability to form plaques on the WT host. By comparing phage titers on *WT* and *supE supF* strains, we found that the fraction of recombinant $\lambda P^{+}S^{+}$ phages after propagation in control (hfq^{+}) cells, was equal to 0.17±0.04%, which was significantly higher than fractions of revertants (spontaneous P^{+} and S^{+} reverse mutants, which appear among mutant phages), achieving a frequency of 0.001% and <0.0001% for λ*P*(am) and λ*S*(am), respectively. When testing efficiency of recombination in Δ*hfq* and ΔCTR hosts, evident influence of the absence of either whole Hfq or its CTR could be observed. Interestingly, the fraction of $\lambda P^{+}S^{+}$ recombinants was about 2-fold lower after propagation of phages in the Δ*hfq* host than in wild-type bacteria, while estimated efficiency of recombination was over 2-times higher in the ΔCTR host relative to the wild-type counterpart

https://doi.org/10.1017/qrd.2022.15 Published online by Cambridge University Press

(Fig. 5B). Therefore, a lack of Hfq results in λ phage recombination inhibition, while in the presence of only Hfq NTR, this process is more efficient in *E. coli.*

As the absence of the CTR could influence Hfq stability and its abundance (Arluison et al., 2004), quantification of Hfq and its CTR-truncated form was performed; no significant differences were observed (Gaffke et al., 2021). Therefore, we conclude that differences in efficiencies of phage M13 replication and phage λ genetic recombination between wild-type bacteria and *hfq* mutants arise from dysfunctions of Hfq in the mutant cells.

Discussion

The results presented in this paper show that, in addition to its role in RNA metabolism, Hfq binds to ssDNA and may therefore play an important role in genetic processes involving ssDNA, including recombination and replication. *In vivo*, the Hfq protein has been discovered as a host factor for bacteriophage replication (Franze de Fernandez et al., 1972). Further studies indicated then that this protein mediates various RNA transactions (Sobrero & Valverde, 2012; Vogel & Luisi, 2011).

Although early studies suggested that Hfq interacts with ssRNA, subsequent experiments indicated that this protein can interact with DNA (Cech et al., 2016). In this report we demonstrate that Hfq interacts also with ssDNA. Note that the role of Hfq in ssDNA binding and remodeling strengthens the general role of bacterial NAPs in similar processes, such as for HU and H-NS/StpA family (Kamashev et al., 2008; Shiraishi et al., 2007; Yang et al., 2019).

We show here that ssDNA binding properties of Hfq are mainly due to its CTR. We observe that CTR binding to ssDNA allows its alignment by forming a parallel helix. This is not the case for ssDNA alone, thus the CTR promotes the formation of this parallel helix probably by changing the pK_A of adenines.

Interestingly, Hfq-CTR has also a propensity to juxtapose two DNA molecules and this is highly suggestive of a role in modulation of efficiency of recombination and/or transformation, as it was formerly shown for another "dsDNA bridging/ssDNA binding" protein, DprA (Mortier-Barriere et al., 2007). To test if such interaction can play a physiological role we have performed efficiency assays for processes that require ssDNA. Our finding that two processes are affected, either positively (M13 replication) or negatively (λ recombination) in the Δ*hfq* mutant might suggest that this is the case. However, any secondary effects of Hfq-mediated changes in regulatory RNA functions could not be excluded in such experimental systems. Therefore, we have also used the

https://doi.org/10.1017/qrd.2022.15 Published online by Cambridge University Press

ΔCTR mutant in which only the NTR of Hfq is present. Surprisingly, we found that effects of the ΔCTR mutation on both M13 replication and λ recombination are more pronounced than in the case of Δ*hfq*, and opposite to those observed in cells completely lacking Hfq. These results corroborate the conclusion that ssDNA binding by Hfq has a physiological relevance. We have also demonstrated that *in vivo* Hfq-CTR stimulates replication of bacteriophage M13 genome, while inhibiting Red recombination. We propose that Hfq-mediated stimulation of M13-replication might relate to changes in ssDNA conformation facilitating alignment of ssDNA in parallel helices, and then the formation of the replication complex, similarly to the mechanism occurring in the Qβ bacteriophage replication. On the other hand, covering ssDNA regions by Hfq during genetic recombination may impair this process due to lower availability of recombining sequences during the exchange process of strands between two DNA molecules.

Recombination efficiency is also controlled by Hfq-CTR which inhibits recombination. Mutant Δ*hfq* cells lacking both the NTR and CTR regions recombine less efficiently in contrast to only CTR deficient cells. WT cells containing Hfq are not substantially more efficient in recombination than Δ*hfq*. Therefore, we hypothesize that effects of the absence of CTR in Δ*hfq* cells might be hidden due to the inability of the NTR to perform its functions. This includes interactions with sRNA and ultimately regulation of gene expression. This definitely makes Hfq an important player to consider in bacterial chromosome structure and gene expression control.

Financial support

This research was supported Singapore Ministry of Education Academic Research Fund (Tier 1 R-144-000-451-114 and Tier 2 MOE-T2EP50121-0003 grants), National Science Center (Poland) (2016/21/N/NZ1/02850 to KK) and University of Gdansk (531-D020-D242-21 to GW). SRCD measurements on DISCO beamline at the SOLEIL Synchrotron were performed under proposal 20200007. SRLD measurements on ASTRID2 synchrotron radiation facility (Aarhus University, Denmark) were performed under proposal ISA-21-102. Campus France is gratefully acknowledged for their financial support of this work through PHC Polonium with Poland 27701VG. This study contributes to the IdEx Université de Paris ANR-18-IDEX-0001. This work was supported by a public grant overseen by the French National research Agency (ANR) as part of the "Investissement d'Avenir" program, through the "ADI 2019" project funded by the IDEX Paris-Saclay, ANR-11-IDEX-0003-02.

https://doi.org/10.1017/qrd.2022.15 Published online by Cambridge University Press

Conflicting of interest declaration

The authors declare no potential conflicts of interest with respect to the research, authorship, and/or publication of this article.

Acknowledgements

We are very grateful to C. Lavelle (MNHN, Paris), P. Dupaigne (IGR, Villejuif, France) and O. Pietrement (U. of Dijon, France) for their contribution to TEM measurements at an early stage of this work and for many fruitful discussions.

Authors' Contributions

KK constructed plasmids and *E. coli* mutant strains, and performed *in vivo* experiments (replication and recombination assessment). JvdM and IY did Optical Microscopy of ssDNA Complexes. FW, VA, NCJ and SVH did SRCD, SRLD and OCD measurement and analysis. AC and ELC did TEM measurements. FG did FTIR measurements. GW and VA concepted the study and supervised the work. All authors participated in the design, interpretation of the studies and analysis of the data and review of the manuscript.

References

Allemand, J. F., Bensimon, D., Jullien, L., Bensimon, A. & Croquette, V. (1997). pH-dependent specific binding and combing of DNA. Biophys J, 73(4), 2064-2070.

Arluison, V., Folichon, M., Marco, S., Derreumaux, P., Pellegrini, O., Seguin, J., Hajnsdorf, E. & Regnier, P. (2004). The C-terminal domain of Escherichia coli Hfq increases the stability of the hexamer. Eur J Biochem, 271(7), 1258-1265.

Bachmann, B. J. (1972). Pedigrees of some mutant strains of Escherichia coli K-12. Bacteriological reviews, 36(4), 525-557.

Banyay, M., Sarkar, M. & Graslund, A. (2003). A library of IR bands of nucleic acids in solution. Biophys Chem, 104(2), 477-488.

Basak, R., Liu, F., Qureshi, S., Gupta, N., Zhang, C., De Vries, R., Van Kan, J. A., Dheen, S. T. & Van Der Maarel, J. R. C. (2019). Linearization and Labeling of Single-Stranded DNA for Optical Sequence Analysis. J Phys Chem Lett, 10(3), 316-321.

https://doi.org/10.1017/qrd.2022.15 Published online by Cambridge University Press

425 Beloin, C., Jeusset, J., Revet, B., Mirambeau, G., Le Hegarat, F. & Le Cam, E. (2003). Contribution
426 of DNA conformation and topology in right-handed DNA wrapping by the Bacillus subtilis LrpC
427 protein. J Biol Chem, 278(7), 5333-5342.

428 Brennan, R. G. & Link, T. M. (2007). Hfq structure, function and ligand binding. Curr Opin
429 Microbiol, 10(2), 125-133.

430 Cech, G. M., Szalewska-Palasz, A., Kubiak, K., Malabirade, A., Grange, W., Arluison, V. &
431 Wegrzyn, G. (2016). The Escherichia Coli Hfq Protein: An Unattended DNA-Transactions
432 Regulator. Front Mol Biosci, 3, 36.

433 Dicko, C., Hicks, M. R., Dafforn, T. R., Vollrath, F., Rodger, A. & Hoffmann, S. V. (2008).
434 Breaking the 200 nm limit for routine flow linear dichroism measurements using UV synchrotron
435 radiation. Biophysical journal, 95(12), 5974-5977.

436 Diestra, E., Cayrol, B., Arluison, V. & Risco, C. (2009). Cellular electron microscopy imaging
437 reveals the localization of the Hfq protein close to the bacterial membrane. PLoS One, 4(12), e8301.

438 Edmondson, S. P. & Johnson, W. C., Jr. (1985). Base tilt of poly[d(A)]-poly[d(T)] and poly[d(AT)]-
439 poly[d(AT)] in solution determined by linear dichroism. Biopolymers, 24(5), 825-841.

440 El Hamoui, O., Yadav, I., Radiom, M., Wien, F., Berret, J.-F., Van Der Maarel, J. R. C. & Arluison,
441 V. (2020). Interactions between DNA and the Hfq Amyloid-like Region Trigger a Viscoelastic
442 Response. Biomacromolecules, 21(9), 3668-3677.

443 Folichon, M., Arluison, V., Pellegrini, O., Huntzinger, E., Regnier, P. & Hajnsdorf, E. (2003). The
444 poly(A) binding protein Hfq protects RNA from RNase E and exoribonucleolytic degradation.
445 Nucleic Acids Res, 31(24), 7302-7310.

446 Fortas, E., Piccirilli, F., Malabirade, A., Militello, V., Trepout, S., Marco, S., Taghbalout, A. &
447 Arluison, V. (2015). New insight into the structure and function of Hfq C-terminus. Biosci Rep,
448 35(2).

449 Franze De Fernandez, M. T., Hayward, W. S. & August, J. T. (1972). Bacterial proteins required
450 for replication of phage Qb ribonucleic acid. J. Biol. Chem., 247, 824-821.

451 Gaffke, L., Kubiak, K., Cyske, Z. & Wegrzyn, G. (2021). Differential Chromosome- and Plasmid-
452 Borne Resistance of Escherichia coli hfq Mutants to High Concentrations of Various Antibiotics.
453 Int J Mol Sci, 22(16), 8886.

454 Geinguenaud, F., Calandrini, V., Teixeira, J., Mayer, C., Liquier, J., Lavelle, C. & Arluison, V.
455 (2011). Conformational transition of DNA bound to Hfq probed by infrared spectroscopy. Phys
456 Chem Chem Phys, 13(3), 1222-1229.

457 Gleghorn, M. L., Zhao, J., Turner, D. H. & Maquat, L. E. (2016). Crystal structure of a poly(rA)
458 staggered zipper at acidic pH: evidence that adenine N1 protonation mediates parallel double helix
459 formation. Nucleic Acids Res, 44(17), 8417-8424.

460 Goldberg, A. R. & Howe, M. (1969). New mutations in the S cistron of bacteriophage lambda
461 affecting host cell lysis. Virology, 38(1), 200-202.

462 Gottesman, S. (2019). Trouble is coming: Signaling pathways that regulate general stress responses
463 in bacteria. The Journal of biological chemistry, 294(31), 11685-11700.

https://doi.org/10.1017/qrd.2022.15 Published online by Cambridge University Press

Hansma, H. G., Sinsheimer, R. L., Li, M. Q. & Hansma, P. K. (1992). Atomic force microscopy of single- and double-stranded DNA. Nucleic Acids Res, 20(14), 3585-3590.

Holm, A. I., Munksgaard Nielsen, L., Vronning Hoffmann, S. & Brondsted Nielsen, S. (2012). On the formation of the double helix between adenine single strands at acidic pH from synchrotron radiation circular dichroism experiments. Biopolymers, 97(7), 550-557.

Holm, A. I. S., Nielsen, L. M., Hoffmann, S. V. & Nielsen, S. B. (2010). Vacuum-ultraviolet circular dichroism spectroscopy of DNA: a valuable tool to elucidate topology and electronic coupling in DNA. Physical chemistry chemical physics : PCCP, 12(33), 9581-9596.

Jensen, K. F. (1993). The Escherichia coli K-12 "wild types" W3110 and MG1655 have an rph frameshift mutation that leads to pyrimidine starvation due to low pyrE expression levels. J Bacteriol, 175(11), 3401-3407.

Jiang, K., Zhang, C., Guttula, D., Liu, F., Van Kan, J. A., Lavelle, C., Kubiak, K., Malabirade, A., Lapp, A., Arluison, V. & Van Der Maarel, J. R. (2015). Effects of Hfq on the conformation and compaction of DNA. Nucleic Acids Res, 43(8), 4332-4341.

Kamashev, D., Balandina, A., Mazur, A. K., Arimondo, P. B. & Rouviere-Yaniv, J. (2008). HU binds and folds single-stranded DNA. Nucleic Acids Res, 36(3), 1026-1036.

Kavita, K., Zhang, A., Tai, C. H., Majdalani, N., Storz, G. & Gottesman, S. (2022). Multiple in vivo roles for the C-terminal domain of the RNA chaperone Hfq. Nucleic Acids Res.

Kenney, L. J. (2019). The role of acid stress in Salmonella pathogenesis. Curr Opin Microbiol, 47, 45-51.

Link, T. M., Valentin-Hansen, P. & Brennan, R. G. (2009). Structure of Escherichia coli Hfq bound to polyriboadenylate RNA. Proc Natl Acad Sci U S A, 106(46), 19292-19297.

Majdalani, N., Cunning, C., Sledjeski, D., Elliott, T. & Gottesman, S. (1998). DsrA RNA regulates translation of RpoS message by an anti-antisense mechanism, independent of its action as an antisilencer of transcription. Proc Natl Acad Sci U S A, 95(21), 12462-12467.

Malabirade, A., Jiang, K., Kubiak, K., Diaz-Mendoza, A., Liu, F., Van Kan, J. A., Berret, J. F., Arluison, V. & Van Der Maarel, J. R. C. (2017a). Compaction and condensation of DNA mediated by the C-terminal domain of Hfq. Nucleic Acids Res, 45(12), 7299-7308.

Malabirade, A., Morgado-Brajones, J., Trepout, S., Wien, F., Marquez, I., Seguin, J., Marco, S., Velez, M. & Arluison, V. (2017b). Membrane association of the bacterial riboregulator Hfq and functional perspectives. Sci Rep, 7(1), 10724.

Malabirade, A., Partouche, D., El Hamoui, O., Turbant, F., Geinguenaud, F., Recouvreux, P., Bizien, T., Busi, F., Wien, F. & Arluison, V. (2018). Revised role for Hfq bacterial regulator on DNA topology. Sci Rep, 8(1), 16792.

Molan, K. & Zgur Bertok, D. (2022). Small Prokaryotic DNA-Binding Proteins Protect Genome Integrity throughout the Life Cycle. Int J Mol Sci, 23(7).

Mortier-Barriere, I., Velten, M., Dupaigne, P., Mirouze, N., Pietrement, O., Mcgovern, S., Fichant, G., Martin, B., Noirot, P., Le Cam, E., Polard, P. & Claverys, J. P. (2007). A key presynaptic role in transformation for a widespread bacterial protein: DprA conveys incoming ssDNA to RecA. Cell, 130(5), 824-836.

https://doi.org/10.1017/qrd.2022.15 Published online by Cambridge University Press

Mosberg, J. A., Lajoie, M. J. & Church, G. M. (2010). Lambda red recombineering in Escherichia coli occurs through a fully single-stranded intermediate. Genetics, 186(3), 791-799.

Nordén, B., Rodger, A. & Daffron, T. (2010). Linear Dichroism and Circular Dichroism A Textbook on Polarized-Light Spectroscopy, pp. 317-370. Cambridge: RCS Publishing

Oakley, A. J. (2019). A structural view of bacterial DNA replication. Protein science : a publication of the Protein Society, 28(6), 990-1004.

Orans, J., Kovach, A. R., Hoff, K. E., Horstmann, N. M. & Brennan, R. G. (2020). Crystal structure of an Escherichia coli Hfq Core (residues 2-69)-DNA complex reveals multifunctional nucleic acid binding sites. Nucleic Acids Res, 48(7), 3987-3997.

Patterson, T. A. & Dean, M. (1987). Preparation of high titer lambda phage lysates. Nucleic acids research, 15(15), 6298.

Piazza, A. & Heyer, W.-D. (2019). Moving forward one step back at a time: reversibility during homologous recombination. Current genetics, 65(6), 1333-1340.

Rajkowitsch, L. & Schroeder, R. (2007). Dissecting RNA chaperone activity. Rna, 13(12), 2053-2060.

Salivar, W. O., Tzagoloff, H. & Pratt, D. (1964). Some physical-chemical and biological properties of the rod-shaped coliphage M13. Virology, 24, 359-371.

Sharan, S. K., Thomason, L. C., Kuznetsov, S. G. & Court, D. L. (2009). Recombineering: a homologous recombination-based method of genetic engineering. Nature protocols, 4(2), 206-223.

Shiraishi, K., Ogata, Y., Hanada, K., Kano, Y. & Ikeda, H. (2007). Roles of the DNA binding proteins H-NS and StpA in homologous recombination and repair of bleomycin-induced damage in Escherichia coli. Genes Genet Syst, 82(5), 433-439.

Shulman, L. M. & Davidson, I. (2017). Viruses with Circular Single-Stranded DNA Genomes Are Everywhere! Annual review of virology, 4(1), 159-180.

Sobrero, P. & Valverde, C. (2012). The bacterial protein Hfq: much more than a mere RNA-binding factor. Crit Rev Microbiol, 38(4), 276-299.

Su, X.-C., Wang, Y., Yagi, H., Shishmarev, D., Mason, C. E., Smith, P. J., Vandevenne, M., Dixon, N. E. & Otting, G. (2014). Bound or free: interaction of the C-terminal domain of Escherichia coli single-stranded DNA-binding protein (SSB) with the tetrameric core of SSB. Biochemistry, 53(12), 1925-1934.

Sutherland, J. C. (2009). Measurement of Circular Dichroism and Related Spectroscopies with Conventional and Synchrotron Light Sources: Theory and Instrumentation. In Modern Techniques for Circular Dichroism and Synchrotron Radiation Circular Dichroism Spectroscopy, B.A Wallace, R.W. Janes (Eds.), pp. 19-72.

Taghbalout, A., Yang, Q. & Arluison, V. (2014). The Escherichia coli RNA processing and degradation machinery is compartmentalized within an organized cellular network. Biochem J, 458(1), 11-22.

Taillandier, E. & Liquier, J. (2002). Vibrationnal spectroscopy of nucleic acids: Willey § sons.

Takada, A., Wachi, M., Kaidow, A., Takamura, M. & Nagai, K. (1997). DNA binding properties of the *hfq* gene product of *Escherichia coli*. Biochem. Biophys. Res. Com., 236, 576-579.

https://doi.org/10.1017/qrd.2022.15 Published online by Cambridge University Press

Tolstorukov, M. Y., Virnik, K. M., Adhya, S. & Zhurkin, V. B. (2005). A-tract clusters may facilitate DNA packaging in bacterial nucleoid. Nucleic Acids Res, 33(12), 3907-3918.

Vogel, J. & Luisi, B. F. (2011). Hfq and its constellation of RNA. Nat Rev Microbiol, 9(8), 578-589.

Wegrzyn, G., Wegrzyn, A., Konieczny, I., Bielawski, K., Konopa, G., Obuchowski, M., Helinski, D. R. & Taylor, K. (1995). Involvement of the host initiator function dnaA in the replication of coliphage lambda. Genetics, 139(4), 1469-1481.

Wien, F., Geinguenaud, F., Grange, W. & Arluison, V. (2021). SRCD and FTIR Spectroscopies to Monitor Protein-Induced Nucleic Acid Remodeling. Methods in molecular biology, RNA Remodeling Proteins (2209), 87-108.

Wien, F., Martinez, D., Le Brun, E., Jones, N. C., Vronning Hoffmann, S., Waeytens, J., Berbon, M., Habenstein, B. & Arluison, V. (2019). The Bacterial Amyloid-Like Hfq Promotes In Vitro DNA Alignment. Microorganisms, 7(12).

Wiggins, P. A., Dame, R. T., Noom, M. C. & Wuite, G. J. (2009). Protein-mediated molecular bridging: a key mechanism in biopolymer organization. Biophys J, 97(7), 1997-2003.

Wilusz, C. J. & Wilusz, J. (2013). Lsm proteins and Hfq: Life at the 3' end. RNA Biol, 10(4), 592-601.

Woolley, A. T. & Kelly, R. Y. (2001). Deposition and characterization of extended single strand DNA molecules on surface. Nano letters, 7, 345-348.

Yadav, I., Rosencrans, W., Basak, R., Van Kan, J. A. & Van Der Maarel, J. R. C. (2020). Intramolecular dynamics of dsDNA confined to a quasi-one-dimensional nanochanne. Phys. Rev. Research 2, 013294.

Yang, D., Kong, Y., Sun, W., Kong, W. & Shi, Y. (2019). A Dopamine-Responsive Signal Transduction Controls Transcription of Salmonella enterica Serovar Typhimurium Virulence Genes. mBio, 10(2).

Zawilak-Pawlik, A., Nowaczyk, M. & Zakrzewska-Czerwinska, J. (2017). The Role of the N-Terminal Domains of Bacterial Initiator DnaA in the Assembly and Regulation of the Bacterial Replication Initiation Complex. Genes, 8(5).

https://doi.org/10.1017/qrd.2022.15 Published online by Cambridge University Press

Legends to the figures

Figure 1. ssDNA coating by Hfq (A1) Montages of ssDNA coated with Hfq or its truncated forms. Molecules are stained with YOYO-1 and stretched on the flat surface by molecular combing. *Scale bar 5 μm*. The corresponding measured extension for combed molecules are also given. Note that the molar concentration of CTR is kept six times higher than hexameric-HFq to maintain the stoichiometric ratio. (B) Histogram of ssDNA molecules imaged in combing (orange, 28 molecules) and inside nanofluidic channel (blue, 39 molecules). The average extension for the combing experiment is 25±2 μm and in the nanofluidic channel is 15±2 μm. (C) TEM evidence of Hfq-ssDNA binding. ΦX174 ssDNA virions were incubated in presence of CTR. Before incubation, virions ssDNA is difficult to visualize (sub-panel A1). CTR binding to ssDNA ΦX174 allows the spreading of some region of the DNA, while others are strongly bridged (sub-panels B1 and B2). In this case the CTR causes the association of several ΦX174 that cannot be differentiated and the length of the viral DNA cannot be measured. *Scale bars: 200nm.*

Figure 2. (A) Structure characterization of ssDNA complexed to Hfq-CTR by SRCD spectroscopy. Spectra of DNA in the absence (red) and presence of CTR (blue). CTR alone (green). The dotted spectrum represents the theoretical sum of individual spectra of the DNA and CTR. The measured spectrum of the complex is significantly different compared to the DNA+peptide theoretical spectra, indicating an conformational change of the complexed ssDNA. Note that the same analysis with the full-length protein was impractical due to the low solubility of the protein. Inset: model of parallel DNA (Gleghorn et al., 2016).

https://doi.org/10.1017/qrd.2022.15 Published online by Cambridge University Press

Figure 3. (A) FTIR transmission spectrum of ssDNA in the presence of Hfq CTR. The ribose stays in C2'-endo since we observe the typical bands at 840 and 970 cm^{-1}. (B) FTIR transmission spectrum of ssDNA in the presence of CTR. The band observed at 1658 cm^{-1}, absent in dA_{59} alone, the shift from 932 to 947 cm^{-1} and the net decrease of the band intensity at 1089 cm^{-1} indicates that a parallel helix is formed by dA_{59} when bound to CTR.

Figure 4. LD signal (A) and absorbance spectra (B) of the complex dA_{59}:CTR (blue), dA_{59} (red) and Hfq-CTR (green). Spectra were measured with a sample pathlength of 0.5 mm and rotation speed of the Couette flow cell of 3000 rpm. (C) SRLD analysis of the same complex measured in a classic 0.024 mm pathlength cell, rotating the cell holder every 90°. The overall shape of the spectra is conserved with maxima and minima in the same positions compare to (A). Amplitude differences are most likely due to differences of the experiments, with a less perfect alignment of the sample in the classic cell.

Figure 5. (A) Development of bacteriophage M13 in *E. coli*. The presented results indicate mean values from three experiments with error bars indicating SD. Symbols (#) and (*) indicate statistically significant differences (p<0.05 in the t-test) between results obtained for hfq^+ and Δ*hfq*, and hfq^+ and ΔCTR, respectively. (B) Efficiency of recombination between λ bacteriophage genomes in E. coli. The presented results show mean values from three experiments with error bars indicating SD. Value of 100% represents fraction of λP^+S^+ recombinants appearing after infection of the hfq^+ host cells with λ*cI857S7*(am) and λ*b519imm21susP* phages which was equal to 0.17±0.04%. Symbols (*) indicate statistically significant differences (p<0.05 in the t-test) between results obtained for hfq^+ and either Δ*hfq* or ΔCTR hosts.

https://doi.org/10.1017/qrd.2022.15 Published online by Cambridge University Press

621 **Figure 1**

A

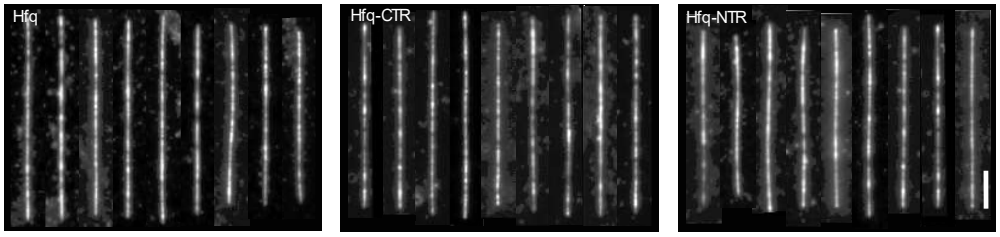

complex	Stretch (μm)	Number of molecules
Hfq (hexamer):base 1:200	25 ± 2	28
Hfq-CTR:base 6:200	25 ± 2	28
Hfq-NTR (hexamer):base 1:200	24 ± 2	24

B

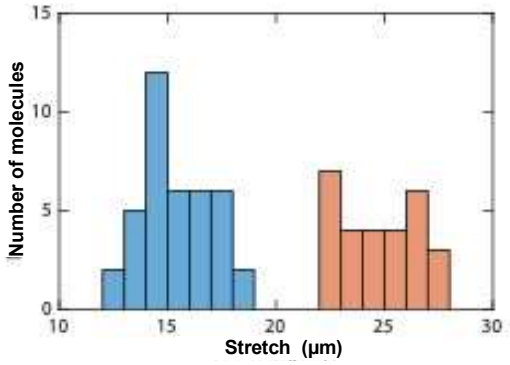

622

623

https://doi.org/10.1017/qrd.2022.15 Published online by Cambridge University Press

Figure 2

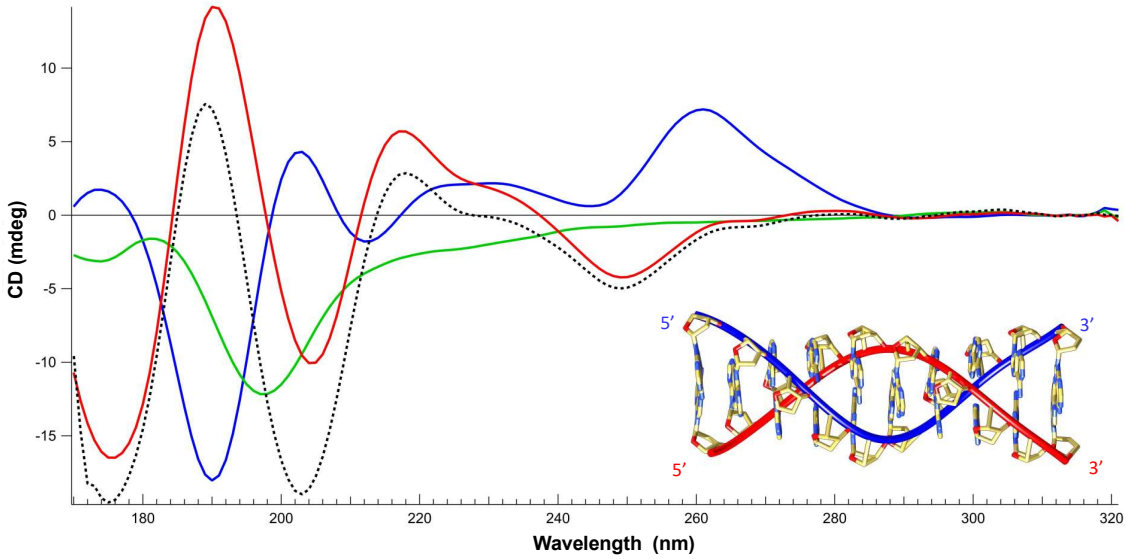

https://doi.org/10.1017/qrd.2022.15 Published online by Cambridge University Press

628 **Figure 3**

629

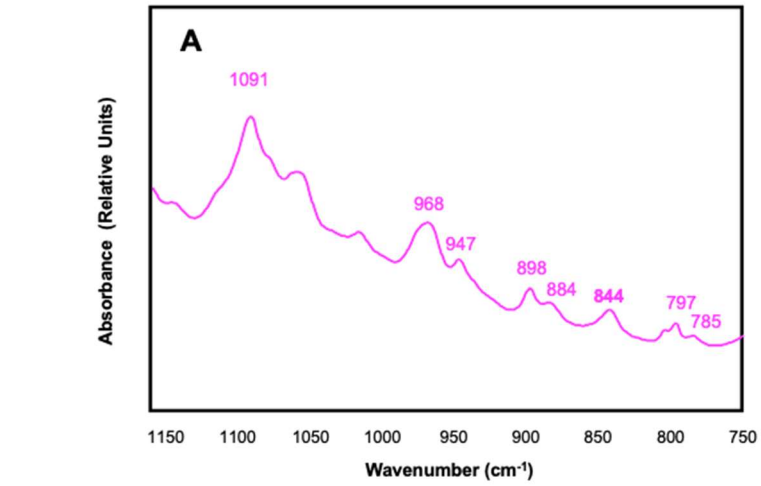

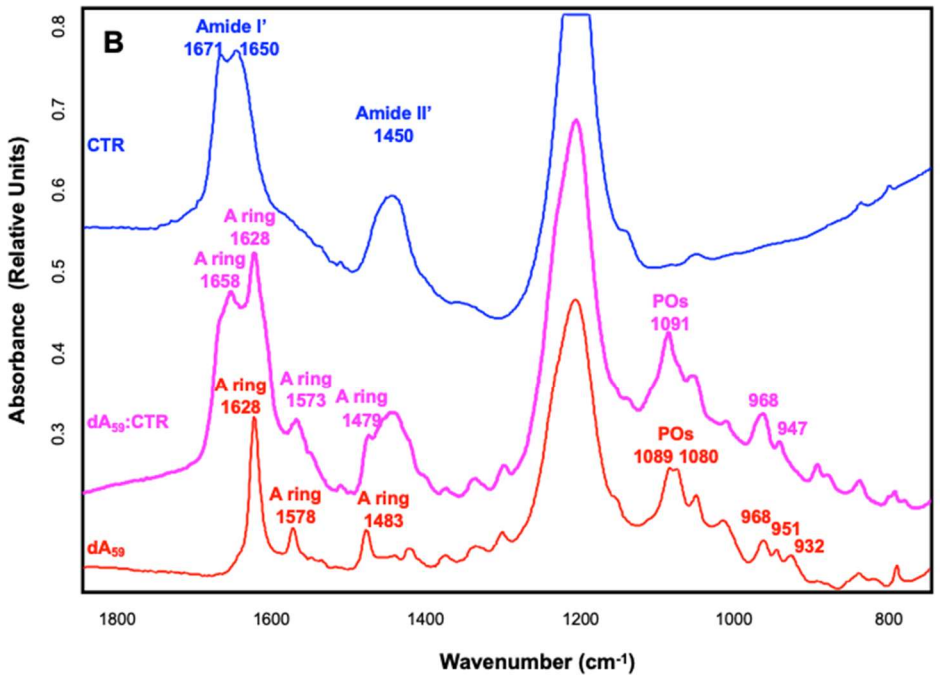

630

631

https://doi.org/10.1017/qrd.2022.15 Published online by Cambridge University Press

632 **Figure 4**

633

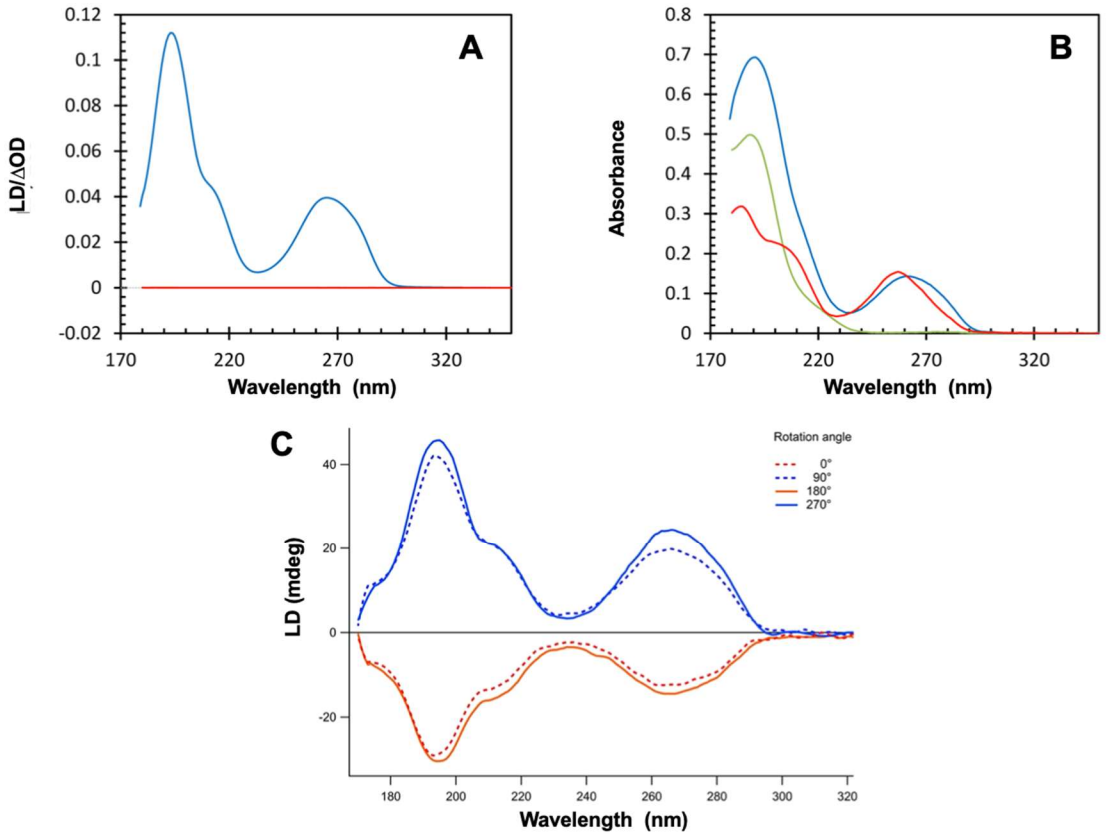

634

635

https://doi.org/10.1017/qrd.2022.15 Published online by Cambridge University Press

636 **Figure 5**

637

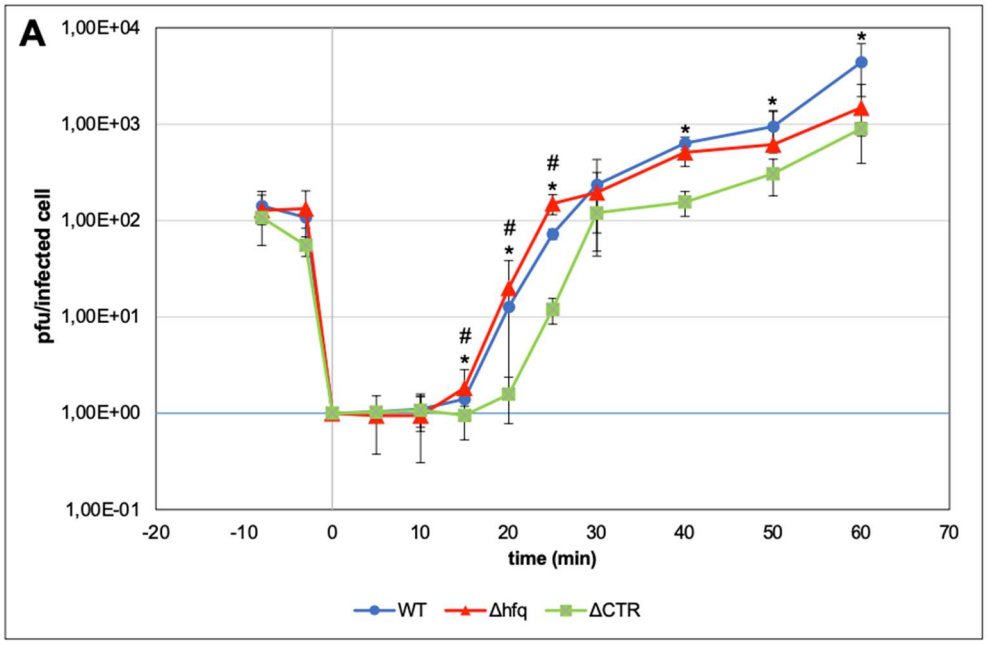

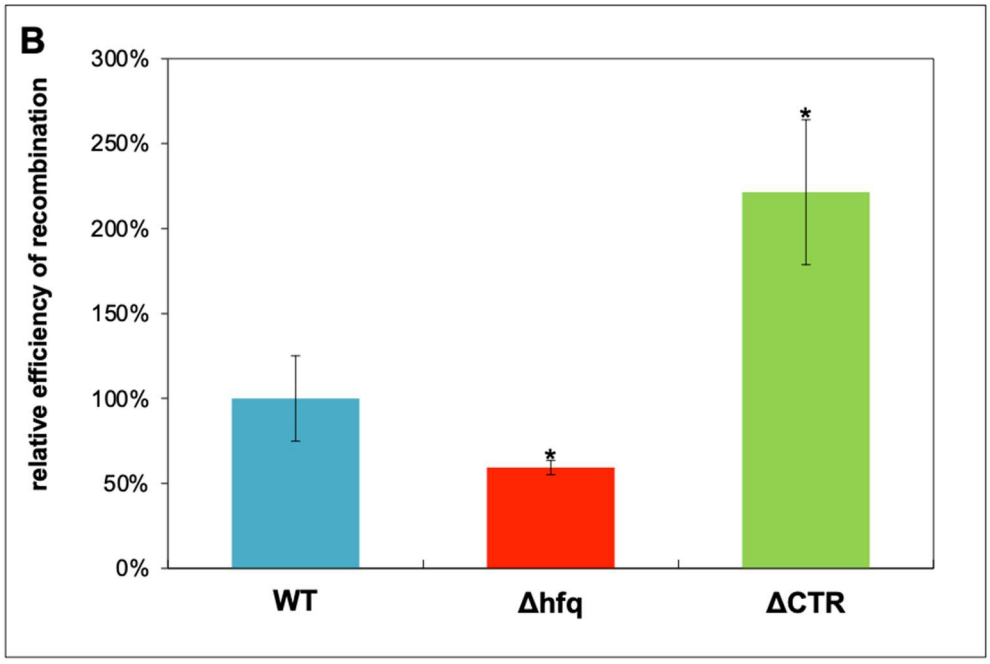

638

https://doi.org/10.1017/qrd.2022.15 Published online by Cambridge University Press